Gamma-ray production from resonant betatron oscillations in plasma wakes.

S. Cipiccia*[a], M. R. Islam [a], B. Ersfeld [a], G. H. Welsh [a], E. Brunetti [a], G. Vieux [a], X. Yang [a], S. M. Wiggins [a], P. Grant [a], D. Reboredo Gil [a], D. W. Grant [a] , R.P. Shanks[b], R. C. Issac[c], M.P. Anania[d], D. Manueski[e], R. Montgomery[e], G. Smith[e], M. Hoek[e], D. Hamilton[e], D. Symes[g], P.P. Rajeev[g], V. O'Shea[e], J.M. Dias[f], N. R. C. Lemos[h], and D. A. Jaroszynski **[a]

[a]Department of Physics, University of Strathclyde, 107 Rottenrow East, Glasgow, G4 0NG, UK

[b]AMS Laboratory, Scottish Enterprise Technology Park Glasgsow G75 0QF

[c] Mar Athanasius College, Kothamanalam, Kerala, India

[d] INFN, Istituto Nazionale di Fisica Nucleare, Frascati, Italy

[e] University of Glasgow, Kelvin Building, Glasgow G12 8QQ

[f]GoLP/Instituto de Plasma e Fusao Nuclear, Instituto Superior Tecnico, Avenida Rovisco Pais 1049-001 Lisbon Portucal

[g] Central Laser Facility, Science and Technology Facilities Council, Rutherford Appleton Laboratory, Harwell Science and Innovation Campus, Didcot OX110QX, UK

[h] UCLA, Westwood Plaza, Los Angeles CA 90095-1594, US

ABSTRACT

The laser-plasma wakefield accelerator is a novel ultra-compact particle accelerator. A very intense laser pulse focused onto plasma can excites plasma density waves. Electrons surfing these waves can be accelerated to very high energies with unprecedented accelerating gradients in excess of 1 GV/cm. While accelerating, electrons undergo transverse betatron oscillations and emit synchrotron-like x-ray radiation into a narrow on-axis cone, which is enhanced when electrons interact with the electromagnetic field of the laser. In this case, the laser can resonantly drive the electron motion, lading to direct laser acceleration. This occurs when the betatron frequency matches the Doppler down-shifted frequency of the laser. As a consequence, the number of photons emitted is strongly enhanced and the critical photon energy is increases to 100's of keV.

Keywords: betatron radiation, resonance, laser, plasma accelerator

1. INTRODUCTION

In a laser-plasma wakefield accelerator[1] a high intensity laser is focused into plasma and its ponderomotive force displaces the electrons from higher intensity regions, while heavier ions are relatively unperturbed, which causes charge separation. Displaced electrons are attracted back by the electrostatic force of the ions and start oscillating around the laser propagation axis at the plasma frequency $\omega_p = \sqrt{\frac{n_p e^2}{m_e \varepsilon_0}}$, which produces a plasma density wave, with n_p the plasma density, m_e the electron mass, e the electron charge and ε_0 the vacuum permittivity. For an intense laser pulse with a length approximately equal to the plasma wavelength, electrons are self-injected into the wake. The plasma wake assumes the shape of plasma cavities or "bubbles" (Figure 1). This highly non-linear regime (so-called "bubble regime") was explored numerically for the first time in 2002 by Pukhov and Meyer-ter-Vehn[2]. Wave breaking gives rise to self-injection at the rear of the bubble where injected electrons experience an accelerating gradient in excess of 100 GV/m[3-5]. Electrons accelerate until they reach the centre of the bubble, beyond which they decelerate. The accelerating length is also called the dephasing length.

To estimate the electric field experienced by the electrons trapped inside the cavity, the bubble can be approximated as a sphere moving along the laser axis z, with velocity equal to the group velocity of the laser v_g. Invoking Gauss' law, the electric potential inside the bubble is:

*silvia.cipiccia@strath.ac.uk
** d.a.jaroszynski@strath.ac.uk

$$\Phi = \frac{en_e}{\varepsilon_0}\left(\frac{R_b^2}{6} - \frac{r^2}{6}\right), \quad (1)$$

where R_b is the bubble radius, $r^2 = x^2 + y^2 + \xi^2$ and $\xi = z - v_g t$ is the co-moving coordinate along the laser propagation axis. The corresponding force is:

$$\vec{F}_b = -\mathrm{e}\nabla\Phi. \quad (2)$$

Electrons injected into the bubble with a non-zero transverse momentum undergo transverse oscillations due to the ion background, while accelerated longitudinally. Considering a simple model of a single electron propagating inside an ion channel, the transverse restoring force is:

$$\vec{F}_{res} = -m_e\omega_p^2\vec{r}_\perp/2. \quad (3)$$

The electron oscillates with a betatron frequency given by:

$$\omega_\beta = \omega_p/\sqrt{2\gamma}, \quad (4)$$

where γ is the Lorentz factor. The oscillatory motion is analogous to the motion of electrons inside a wiggler[6] with periodicity λ_β and strength parameter (normalized transverse momentum):

$$a_\beta = \gamma\theta = \gamma k_\beta r_\beta, \quad (5)$$

where θ is the maximum deflection angle of the trajectory, k_β is the betatron wavenumber and r_β the betatron oscillation amplitude. The properties of the betatron emission depend strongly on a_β. If $a_\beta < 1$ the electrons primarily emit at the fundamental frequency, which is the Doppler shifted betatron frequency:

$$\omega_f = \omega_\beta 2\gamma^2 = \sqrt{2}\gamma^{3/2}\omega_p. \quad (6)$$

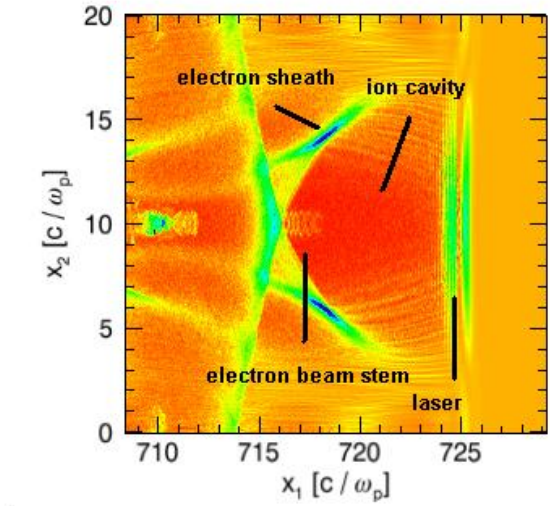

Figure 1: Bubble picture obtained from OSIRIS[7] simulation showing the three different density regions that identify the bubble: the ion cavity behind the laser pulse, the high density electron sheath and the trapped electrons forming a stem.

For $a_\beta > 1$ the amplitude of the oscillation grows and higher harmonics are radiated. The spectral intensity grows up to the critical frequency

$$\omega_c = \frac{3c\gamma^3}{2R}, \quad (7)$$

where c is the speed of light and $R = k_\beta^2/r_\beta$ is the effective radius of curvature. The number of photons emitted per electrons at every betatron oscillation is:

$$N_{phot} = \frac{2\pi}{9}\alpha a_{\beta,} \tag{8}$$

where $\alpha = 1/137$ is the fine structure constant. During acceleration the amplitude of the oscillation decreases as $\gamma^{-1/4}$. The damping of the oscillation amplitude during the acceleration is shown in Figure 2.

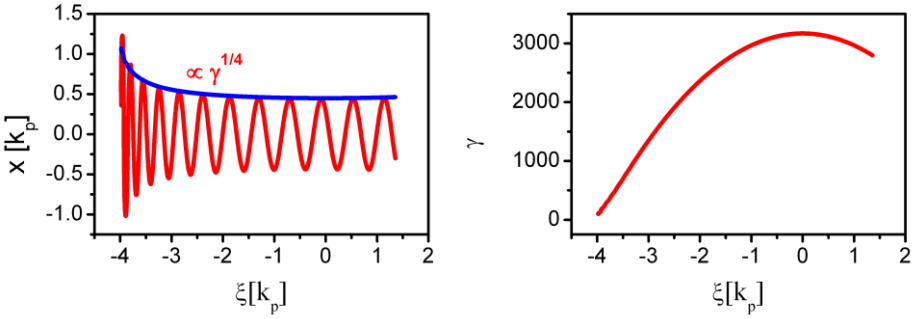

Figure 2: Evolution of the electron trajectory (l.h.s.) and electron Lorentz factor (r.h.s.) in the bubble regime as calculated analytically assuming a spherical bubble and a plasma density of $2\text{x}10^{18}$ cm^{-3}. The oscillation amplitude evolves as $\gamma^{-1/4}$.

2. HARMONICALLY RESONANT BETATRON MOTION

During the acceleration inside the bubble, the electron beam can interact with the laser pulse and experience its electromagnetic field. When this occurs the dynamics of the electrons are dramatically altered. If A is the laser vector potential, the Lorentz force due to the laser field is:

$$\vec{F}_L = -e\left(-\frac{\partial \vec{A}}{\partial t} + \vec{v} \times \left(\nabla \times \vec{A}\right)\right), \tag{9}$$

and the total force acting on the electrons becomes:

$$\vec{F}_b = -e\left(\nabla\Phi - \frac{\partial \vec{A}}{\partial t} + \vec{v} \times \left(\nabla \times \vec{A}\right)\right). \tag{10}$$

Assuming the laser propagates along z and is linearly polarized in y, its vector potential can be written as:

$$\vec{A} = \hat{y}A_0 \mathrm{e}^{-\frac{(t-z/v_g)^2}{2\tau^2}} \mathrm{e}^{-\frac{(x^2+y^2)}{2\sigma^2}} \cos(k_0 z - \omega_0 t). \tag{11}$$

The transverse component of the total force acting of the electrons can be written as:

$$F_{by} = \frac{dp_y}{dt} = \frac{d}{dt}(m_e\gamma\dot{y}) = m_e\gamma\ddot{y} + m_e\dot{\gamma}\dot{y} = -\omega_\beta^2 y + F_{Ly}$$

$$\ddot{y} + \Gamma\dot{y} + \omega_\beta^2 \frac{2}{3} y = \frac{F_{Ly}}{m_e\gamma} \quad . \tag{12}$$

This is the equation of a damped, driven harmonic oscillator, where $\Gamma = \dot{\gamma}/\gamma$ is the damping factor due to the relativistic mass increase[8,9]. The dependence of ω_β on γ leads to a shift of the resonance frequency on a slow timescale. The oscillation amplitude grows considerably when $\Gamma < \omega_\beta$ and the Doppler shifted laser frequency as seen by the electrons, $\tilde{\omega} = \omega_0\left(\frac{1}{2\overline{\gamma_z}^2} + \frac{1}{2\gamma_g'^2}\right)$, drifts into resonance with a harmonic of the betatron oscillation frequency, which occurs when

$\tilde{\omega} = l\omega_\beta$, where l is the harmonic number. At dephasing, when the electron beam reaches the middle of the bubble, Γ vanishes and the betatron amplitude increases suddenly.

The harmonic resonant regime has been observed in simulations[8] using the OSIRIS PIC code, as shown in Figure 3. Electrons that are injected into the rear of the bubble (Figure 3b) undergo betatron oscillations that are damped at a rate given by Γ (> 0). At dephasing $\Gamma \approx 0$ and when resonance occurs, there is a sudden growth of the betatron oscillation amplitude, which can approach the bubble radius. The laser phase experienced by electrons at their longitudinal positions are similar, which causes the electron trajectories to coalesce[10], as is observed in Figure 3c-d. As the betatron frequency decreases with increasing mean axial velocity, it stays in resonance with Doppler shifted laser frequency only for a short time and then it slips to one half, one third etc., sub-harmonics if γ keeps growing. Since the resonance at the fundamental cannot be maintained for a long time as γ grows, this is not sufficient to explain a large growth in a_β. The inclusion of the damping term in the equation of motion introduces both even and odd harmonics, allowing the resonance between the Doppler-shifted laser and the betatron harmonics to persist, thus allowing a_β to grow to large values.

High r_β and a_β values correspond to a high critical frequency of the betatron spectrum, which also leads to an enhancement of the number of photons emitted per electron. The betatron radiation spectrum in the harmonically resonant regime can stretch into the MeV range, which also strongly enhances the source brightness.

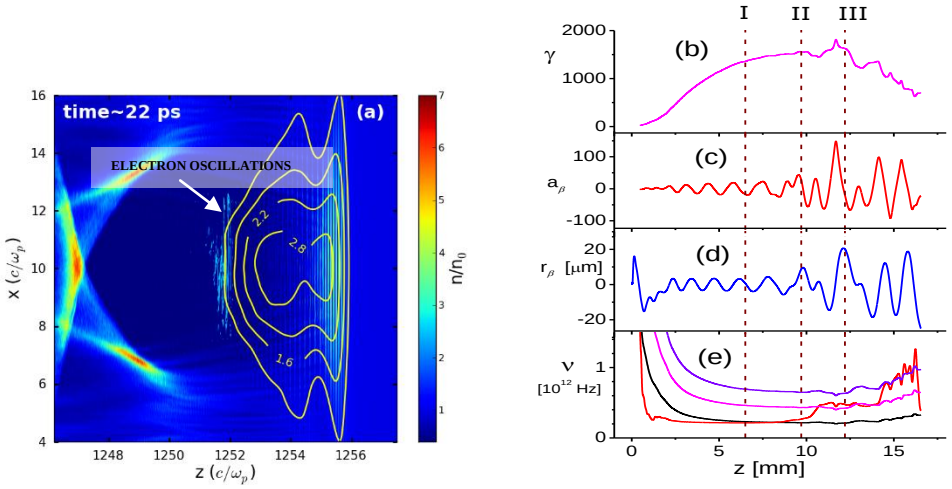

Figure 3: OSIRIS simulations of laser-driven betatron oscillations from Ref 8: l.h.s snapshot of the electron distribution and electron beam trajectories for the non-resonant inside the bubble. The amplitude of the oscillations grows as the electrons approach the head of the bubble. r.h.s. Trajectory of one electron showing evolution of γ b), a_β c), r_β d), and frequencies e).

3. EXPERIMENTAL EVIDENCE OF HARMONIC BETATRON RESONANCE

Being able to detect and characterize the betatron spectrum on every shot enables a better understanding of its role in the acceleration process, which is important in the development of tuneable, compact, particle and radiation sources. Experiments have shown that betatron radiation is bright, spatially coherent[11] and tuneable in the keV range, with a peak energy in the 1-10 keV range. However, as discussed in the previous section, the interaction of electrons with the laser pulse can amplify the betatron motion leading to an increase in the energy of emitted photons, which can extend to several MeV. This also increases the number of photons emitted per electron by an order of magnitude. The wide energy range and high flux makes the betatron radiation spectrum difficult to measure directly in a single shot. For a broad energy range, different spectrometers can be used to measure spectra in different energy windows and then reconstruct the spectrum. Compton scattering, on the other hand, can be used to simultaneously compress the energy spectrum[12] while attenuating the flux. The spectrum can be measured in a single shot using an energy resolving pixilated semiconductor detector such as Timepix[13], which makes the system suitable for measurements up to several MeV.

To investigate the potential of betatron emission as a brilliant source of hard X-rays and gamma rays, we have focused a 5 J and 55±5 fs duration laser pulse from the ASTRA-Gemini laser[14] into a preformed plasma waveguide[15] with a plasma density $n_p \approx 1\text{-}2 \times 10^{18}$ cm^{-3} (Figure 4)[8].

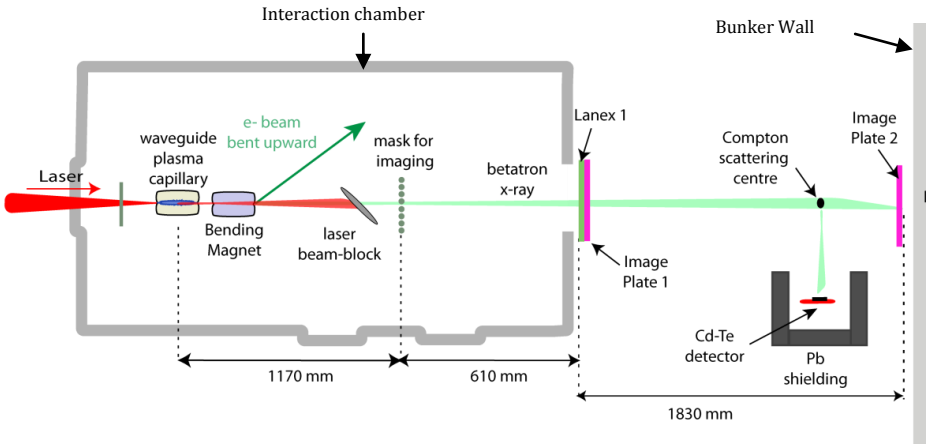

Figure 4: Experimental setup from Ref 8: A F/16 spherical mirror focuses the laser pulse (5 J, 55±5 fs, 800 nm) to a 40±5 μm diameter spot at the entrance of 4 cm long, 300 μm diameter, pre-formed plasma capillary waveguide with an on-axis density of $n_p \approx 2\times10^{18}$ cm^{-3}. The laser beam initially has an intensity of 9×10^{18} Wcm^{-2}. At the end of the interaction chamber Lanex 1 and image plate 1 is used to detect the electron beam deflected by the bending magnet. On the r.h.s.: the x-ray detectors; image plate 2 placed on axis and the CdTe Timepix detector screened behind lead bricks to measure the radiation side-scattered by an aluminium post via the Compton effect.

During the experiment three different regimes (highly damped, and weakly and strongly resonant) have been explored and fully characterized. The regime of operation can be selected using the tuning parameters: laser intensity, laser pulse length, density modulation inside the capillary and controlled injection of electrons.

Highly damped regime:

To explore the highly damped regime a plasma density of $n_p \approx 1.6\times10^{18}$ cm^{-3} is used. In this regime x-rays are expected to be emitted with spectra peaked at a few tens of keV. Since the CdTe detector [13] is not suitable at these x-ray energies because of strong K_α emission at 30 keV from the semiconductor bulk, to measure the x-ray beam divergence and estimate the critical photon energy, an image plate is placed on axis against the Perspex window of the vacuum chamber. A set of metal foils (4 per time), of different thicknesses or material, are placed 93 cm from the capillary exit on the x-ray beam axis. The electron beam is dispersed upward by the bending magnet to avoid irradiating the filters and image plates. Simultaneous measurement of the attenuation through different foils gives a good estimation of both the background noise level and the critical photon energy of the emitted radiation. Using this technique it has been possible to estimate the peaks of the spectra to be around 20±2 keV (as shown in Figure 5[8]), corresponding to a critical photon energy of 60 keV, while the measured x-ray angular divergence is 14 mrad, for 600-700 MeV electrons, which corresponds to $r_\beta \approx 3$ μm and $a_\beta \approx 20$.

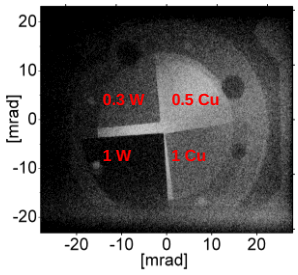

Figure 5 : X-ray image of transmission through metallic filters [0.3 (top left) and 1 mm (bottom left) tungsten foil, 0.5 (top right) and 1 mm (bottom right) copper foil]. Calibrated filter attenuation gives a spectral peak at 20 keV (critical energy of 60±15 keV).

Weakly and strongly resonant regime:

To explore the weakly and strongly resonant regime, a higher density, $n_p \approx 2.0\ 10^{18}$ cm^{-3} has been used. Single shot gamma-ray spectra are recorded using the Compton side scattering technique[12] at 90°. The x-ray spectrum in Figure 6-a peaks at 50 keV (i.e. critical energy of 150 keV). For $n_e = 2\times10^{18}$ cm^{-3}, $\gamma = 1400$, a critical energy of $E_c = 150$ keV, corresponding to $a_\beta = 50$, which matches the values expected for the weakly resonant case (II) shown in Figure 3, where injection occurs later and the electron bunch exits the potential before dephasing and growth in r_β has taken place. In contrast, the peak at 150 keV (i.e. critical energy of 450 keV) shown in Figure 6-b corresponds to a strong resonant interaction with the laser (III) and evolution that has already passed dephasing. Performing the same kind of calculations for the new values $n_e = 2\times10^{18}$ cm^{-3}, $\gamma = 1400$ and $E_c = 450$ keV, we obtain, $a_\beta = 160$. This is what is expected for the strongly resonant case (III) as shown in Figure 3. A summary of the results obtained are reported in Table 3 2. As already pointed out in the previous sections, the agreement between experiment and simulations is good in all the three regimes. It is important to notice that, while switching from one regime to another, the measured electron energy is almost constant ~ 700 MeV. The main difference is that a_β is different for the different cases. Indeed, we expect the most part of the emission to occur close to dephasing when the energy is maximum. And moreover, as predicted in OSIRIS simulations, shown in Figure 3, all three regimes can occur close to dephasing.

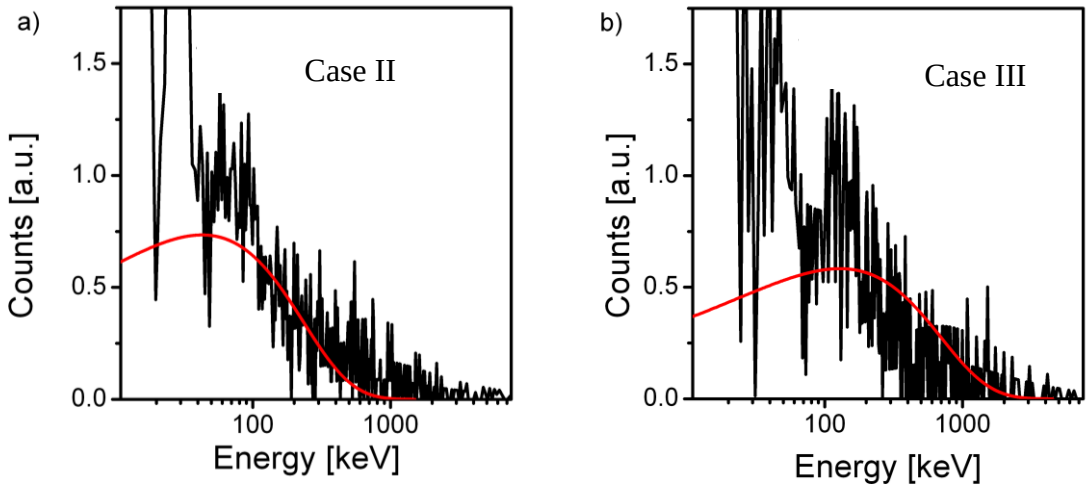

Figure 6: Two of the single shot x-ray spectra[8], from 90° Compton side scattered radiation from a 12 mm Al rod measured with a CdTe semiconductor detector, are overlapped with the predicted synchrotron spectra corresponding to the measured critical photon energies. l.h.s: a spectrum peaking at 50 keV, corresponding to a critical energy of 150 keV, identifies the weakly resonant case II. r.h.s. a spectrum peaking at 150 keV, corresponding to a critical energy of 450 keV, identifies as the strongly resonant case III. During the experiment we recorded in total ~ 20 single shot spectra corresponding to the harmonically resonant regime. The measured

electron energy is 633±70 MeV for both cases. The energy has been estimated from the average over 10 electron spectra obtained before the lanex is removed for the single-shot x-ray measurement.

4. SOURCE SIZE ESTIMATION

The size of a betatron source corresponds to the amplitude of the betatron oscillation. To prove that the gamma rays originate from a very small source size we have used the phase contrast technique.

During the experiment[8] we imaged a grid of copper wires with different thickness (100, 75, 50, 40 and 25 μm diameter), placed 1.17 m from the betatron source inside the vacuum chamber[8]. An imaging plate (FUJI-BAS-MS-2325) is placed 3.6 m from the source. The resolution of the image plate is 50 μm. The image detected in a single shot experiment is shown in Figure 7. To deduce the source size from the recorded image, we compared the experimentally measured wire profiles with calculations carried out for a finite size source[8]. In the calculation we trace the rays from the source to the screen taking into account both attenuation and refraction inside the wires (Figure 8).

A good match for all the different thickness is obtained for a source size of 15 μm, which corresponds to an oscillation amplitude $r_\beta = 7.5$ μm. This matches the predicted oscillation amplitude in the weakly resonant case (II) with OSIRIS.

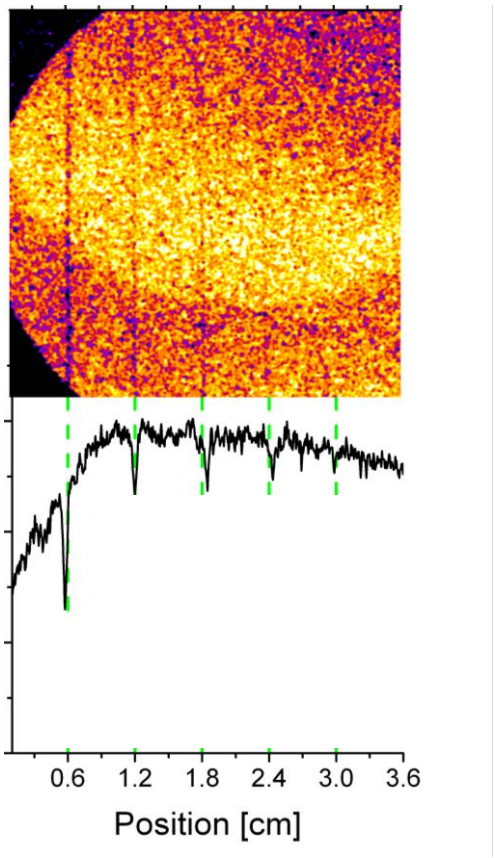

Figure 7: a) Phase contrast image recorded on an image-plate placed close to the bunker wall[8], showing four copper wires of 100, 75, 50 and 40 μm thickness respectively from left to right. Lineout b) shows image profiles where the faint shadow of a fifth 25 μm thick wire is barely visible at position 3 cm. From calculations the expected attenuation without refraction would give a signal about 70% weaker.

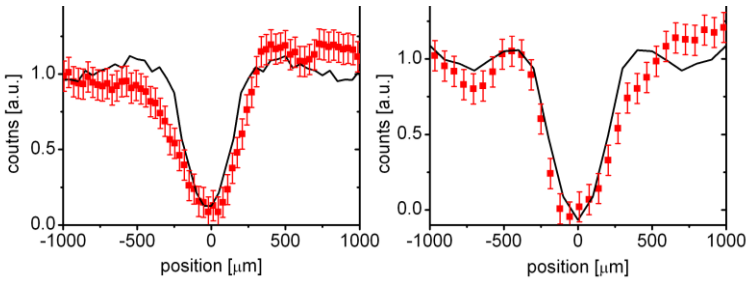

Figure 8: Plots of the shadows cast by the wires (solid squares) compared with data fits (solid lines) consistent with a 15 μm diameter x-ray source size for 75 (l.h.s) and 100 μm (r.h.s)[8]. The calculations have been done assuming an x-ray spectrum distributed over 10 to 100 keV, corresponding to the weakly resonant case. The error bars are given by the standard deviation of the background obtained in the region of the IP alongside the image.

5. CONCLUSION

In conclusion, we have presented experimental evidence of harmonically resonant electron-laser interaction[8] observed in PIC simulations. The highly damped, weakly and strongly resonant regimes have been explored and fully characterized.

The regime of operation can be selected using the tuning parameters: laser intensity, laser pulse length, density modulation inside the capillary and controlled injection of electrons. The success of the experiment relies first of all on a theoretical understanding of the electron-laser interaction process, which has enabled a careful design of the experiment setup and the accurate modelling and understand of the detection system.

Compton side scattering[12] has been used to measure the intense narrow beam of hard x-rays resulting from the betatron motion of high energy electrons. Spectra measured in the strongly resonant regime extend up to several MeV, which is an energy region where currently no synchrotron sources are currentlyavailable.

The x-ray pulse length is estimated to be ≈10 fs from OSIRIS simulations, considering that most photons are emitted when γ is large at resonance. From GEANT4[16] simulations, it has been possible to calculate the x-ray detection efficiency in the Compton side scattering configuration and to estimate the number of incoming photons to be about 5×10^8. After correcting the acquired spectrum by the detection efficiency calculated using GEANT4[16], we obtained the number of photons per unit energy that can be then normalized to 0.1% of the bandwidth (BW). By using a source size value of 20 μm and the pulse length of 10 fs, estimated from OSIRIS simulations, we obtain a peak brilliance in excess of 10^{23} photons/s mrad^2 mm^2 0.1% B.W., which is comparable with the brilliance of a third generation storage ring, but in a spectral range not accessible to synchrotrons. In the strongly resonant regime it should be possible to scale up the resonant betatron source spectra to several MeV with higher laser intensities and lower plasma densities. For example $a_0 = 10$, $n_e = 10^{18}$ cm^{-3} and $r_\beta = R = 34$ μm gives $a_\beta \approx 200$, which will produce photons with a critical energy > 5 MeV and an efficiency ≈1% or larger. Such a source would open up new applications in high contrast imaging of weakly absorbing matter, time-resolved probing of the nucleus and production of medical radio-isotopes through photo-nuclear reactions and dense matter imaging (i.e. probing pellets used in inertial confinement fusion).

ACKNOWLEDGEMENTS

We acknowledge the support of the U.K. EPSRC (EP/J018171/1) and the EC's 7th Framework Programme (LASERLAB-EUROPE no. 284464, the EUCARD-2 project (no. 312453) and the Extreme Light Infrastructure (ELI) project). We also thank D. Clark and T. McCanny for their technical support, without which the project would not have been possible. The authors would like to thank the OSIRIS consortium (UCLA/IST) for the use of OSIRIS.

REFERENCES

[1] Tajima, T. & Dawson, J. M. Phys. Rev. Lett. 43, 267 (1979).

[2] Pukhov, A. & Meyer-Ter-Vehn, J. "Laser wake field acceleration: the highly non-linear broken wave regime". Appl. Phys. B 74, 355-361 (2002).

[3] Mangles, S. P. D. & al., e. "Electron Acceleration from the Breaking of Relativistic Plasma Waves". Nature 431, 535-538 (2004).

[4] Geddes, C. G. R. & al., e. "High Quality Electron Beams from a Laser Wakefield Accelerator Using Plasma-Channel Guiding". Nature 431, 538-541 (2004).

[5] Faure, J. & al., e. "A Laser-Plasma Accelerator Producing Monoenergetic Electron Beams". Nature 431, 541-544 (2004).

[6] Whittum, D. H. "Electromagnetic-Instability of the Ion-Focused Regime". Phys Fluids B-Plasma 4, 730-739 (1992).

[7] Fonseca, R. A. "Lectures Notes". Comput. Sci. 2331, 9 (2002).

[8] Cipiccia, S. *et al.* "Gamma-Rays from Harmonically Resonant Betatron Oscillations in a Plasma Wake". Nat Phys 7, 867-871 (2011).

[9] Nam, I., Hur, M. S., Uhm, H. S., Hafz, N. A. M. & Suk, H. "Controlling the Betatron Oscillations of a Wakefield-Accelerated Electron Beam by Temporally Asymmetric Laser Pulses". Phys Plasmas 18, 043107 (2011).

[10] Nemeth, K. *et al.* "Laser-Driven Coherent Betatron Oscillation in a Laser-Wakefield Cavity". Phys Rev Lett 100, 095002 (2008).

[11] Shah, R. C. *et al.* "Coherence-Based Transverse Measurement of Synchrotron X-ray Radiation from Relativistic Laser-Plasma Interaction and Laser-Accelerated Electrons". Phys Rev E 74, 045401 (2006).

[12] Cipiccia, S. *et al.* "Compton scattering for spectroscopic detection of ultra-fast, high flux, broad energy range X-rays". Review of Scientific Instrument 84 (2013).

[13] Llopart, X., Ballabriga, R., Campbell, M., Tlustos, L. & Wong, W. "Timepix, a 65k Programmable Pixel Readout Chip for Arrival Time, Energy and/or Photon Counting Measurements". Nucl Instrum Meth A 581, 485-494 (2007).

[14] Hooker, C. J. *et al.* "Commissioning the Astra Gemini petawatt Ti:sapphire laser system". 1-2 (2008).

[15] Hooker, S. M. *et al.* "GeV Plasma Accelerators Driven in Waveguides ". Plasma Phys. Control. Fusion 49, B403 (2007).

[16] Agostinelli, S. *et al.* "GEANT4-a Simulation Toolkit". Nucl Instrum Meth A 506, 250-303 (2003).